

Topological phases in nitrogen-doped chevron graphene nanoribbons

Yixuan Gao(高艺璇), Xinxi Zeng(曾新喜), and Ruizi Zhang(张瑞梓)
Citation: Chin. Phys. B, 2026, 35 (**3**): 037103. DOI: 10.1088/1674-1056/ae27b2
http://cpb.iphy.ac.cn; http://iopscience.iop.org/cpb

What follows is a list of articles you may be interested in

First-principles insights into $NaMgPO_3S$ oxysulfide solid electrolyte

Jian Sun(孙健), Shaohui Ding(丁少辉), Daquan Yang(杨大全), Kan Zhang(张侃), and Huican Mao(毛慧灿)
Chin. Phys. B, 2026, 35 (**2**): 027105. DOI: 10.1088/1674-1056/adf17d

First-principles calculations on strain tunable hyperfine Stark shift of shallow donors in Si

Zi-Kai Zhou(周子凯) and Jun Kang(康俊)
Chin. Phys. B, 2025, 34 (**8**): 087102. DOI: 10.1088/1674-1056/addeba

Ab initio prediction of ground-state magnetic ordering and high-pressure magnetic phase transition of uranium mononitride

Jing-Jing Zheng(郑晶晶), Yuxi Chen(陈禹西), Chengxiang Zhao(赵承祥), Junfeng Zhang(张均锋), Ping Zhang(张平), Bao-Tian Wang(王保田), and Jiang-Jiang Ma(马江将)
Chin. Phys. B, 2025, 34 (**8**): 087101. DOI: 10.1088/1674-1056/add4e6

Anomalous ultrafast thermalization of photoexcited carriers in two-dimensional materials induced by orbital coupling

Zhuoqun Wen(文卓群), Haiyu Zhu(诸海渝), Wen-Hao Liu(刘文浩), Zhi Wang(王峙), Wen Xiong(熊稳), and Xingzhan Wei(魏兴战)
Chin. Phys. B, 2025, 34 (**7**): 077103. DOI: 10.1088/1674-1056/adc191

Quantum oscillations and nontrivial topology in unfilled skutterudite $IrSb_3$

Yang Yang(杨扬), Xinyao Li(李鑫垚), Feihong Guan(关飞鸿), Majeed Ur Rehman, Wei Ning(宁伟), Xiangde Zhu(朱相德), and Mingliang Tian(田明亮)
Chin. Phys. B, 2025, 34 (**6**): 067103. DOI: 10.1088/1674-1056/adc7f2

Topological phases in nitrogen-doped chevron graphene nanoribbons

Yixuan Gao(高艺璇)[1,†], Xinxi Zeng(曾新喜)[2], and Ruizi Zhang(张瑞梓)[3,‡]

[1] *State Key Laboratory for Advanced Metals and Materials, University of Science and Technology Beijing, Beijing* 100083, *China*
[2] *School of Mechanical Engineering, University of Science and Technology Beijing, Beijing* 100083, *China*
[3] *National Key Laboratory of Materials for Integrated Circuits, 2020-Xlab, Shanghai Institute of Microsystem and Information Technology, Chinese Academy of Sciences, Shanghai* 201800, *China*

(Received 22 September 2025; revised manuscript received 2 December 2025; accepted manuscript online 4 December 2025)

Researches on one-dimensional topological insulators have garnered significant attention following the discovery of symmetry-protected topological phases in graphene nanoribbons (GNRs). The topological properties of GNRs are modulated by shape modulation, such as altering the width, edge structure, and unit cell termination. Compared to shape modulation, the introduction of foreign atoms doping in the unit cell has proven more practical. However, the impact of doping on topological properties and the underlying mechanisms remain incompletely understood. In this study, nitrogen doping in chevron GNR is utilized to investigate the mechanism of the topological properties with different doping concentrations. The nitrogen doping reduces the intracell hopping parameter, and transforms the GNR from trivial to nontrivial when the doping level reaches eight nitrogen atoms per unit cell. Additionally, the GNR junctions comprising the chevron-GNR and pristine armchair GNRs demonstrate antiferromagnetic exchange coupling. These findings may inform future experimental design of GNR-based electronic devices.

Keywords: one-dimensional topological insulators, nitrogen-doped chevron graphene nanoribbons, density functional theory, junction states, antiferromagnetic spin centers

PACS: 71.15.Mb, 73.40.Lq, 61.48.Gh, 61.82.Fk

DOI: 10.1088/1674-1056/ae27b2 **CSTR:** 32038.14.CPB.ae27b2

1. Introduction

The investigation of topological materials and their distinctive robust in-gap surface or interface states can be traced back to the discovery of the $Bi_{1-x}Sb_x$ family.[1,2] While previous research predominantly focused on three-dimensional (3D)[3,4] and two-dimensional (2D) systems.[5–7] One-dimensional (1D) systems have recently garnered increased attention following the theoretical prediction of symmetry-protected topological phases in graphene nanoribbons (GNRs).[8–11] GNRs exhibit comparable physical behaviors to their higher-dimensional counterparts with reduced complexity, offering substantial potential for realizing nontrivial in-gap states. Recent experimental work has demonstrated a topologically engineered GNR superlattice hosting a 1D array of nontrivial in-gap states.[12–14] The study of 1D topological GNRs with topologically nontrivial states has significant implications for practical applications, including solar cell, spintronics, catalysis as active sites, and topological superconductors.[15–17]

The topological properties of GNRs are determined by the Z_2 invariant, an index of either 0 or 1, indicating two distinct topological classes. The Z_2 invariant correlates with the width, edge shape and terminating crystallographic unit cell of the GNRs.[8] Consequently, the topological properties of GNRs can be manipulated through various methods, including modifications to widths and termination,[8,11,18,19] extending the shape from armchair edge to cove or chevron edge. While previous investigations concentrated on GNRs with different unit cell shapes,[17,20] introducing foreign atom doping while maintaining the unit cell shape has proven more accessible. For instance, nitrogen doping in GNRs typically induces an overall band shift.[21] However, the effect of doping on topological properties and the underlying mechanisms have remained incompletely understood.

In this work, nitrogen doping is introduced in chevron GNR (CGNR) to reduce the intracell hopping parameter and transform the CGNR from trivial to nontrivial when the dopant reaches eight nitrogen atoms per unit cell. The nitrogen atoms are incorporated at the edges to maintain the total electron to be the same. To further utilize the topological states, three superlattices are constructed using two topologically inequivalent segments: 4N-CGNR/8N-CGNR superlattice, 9AGNR/4N-CGNR superlattice and 9AGNR/8N-CGNR superlattice. The analysis reveals that the 9AGNR/4N-CGNR superlattice exhibits type-I band alignment, which indicate that the topological states are around the Fermi level. Density functional theory (DFT) calculations demonstrate that the junction states in this superlattice function as stable spin centers, forming a Heisenberg antiferromagnetic chain. These

†Corresponding author. E-mail: gaoyixuan@ustb.edu.cn
‡Corresponding author. E-mail: rzzhang@mail.sim.ac.cn

© 2026 Chinese Physical Society and IOP Publishing Ltd. All rights, including for text and data mining, AI training, and similar technologies, are reserved.

findings establish a promising framework for experimental realization of robust junction states and further investigation of 1D quantum spin physics.

2. Results and discussion

Recently, a specific type of CGNRs, related to armchair GNRs, has been synthesized through bottom-up self-assembly of molecular building blocks.[21–24] This study examines the topological properties and underlying mechanisms of such GNRs. Three CGNRs with identical unit cell shapes but varying nitrogen atom doping levels are analyzed: pristine chevron GNR (p-CGNR), four nitrogen atoms doped (4N-CGNR) and eight nitrogen atoms doped at the edge in a unit cell of chevron GNR(8N-CGNR), as shown in Fig. 1(a). Although the edge-doped nitrogen atoms maintain consistent total electron counts, they provide an effective method for modifying electronic band structures. As shown in Fig. 1(b), the band structures of these three ribbons exhibit similar band gaps (1.58 eV, 1.58 eV, 1.49 eV for p-, 4N- and 8N-CGNR, respectively). A significant band offset is observed, consistent with previous studies.[21,25] For instance, the valence band maximum (VBM) of the 8N-CGNR is 0.2 eV lower in energy than the VBM of the 4N-CGNR; similarly, a 0.3 eV shift applies to the conduction band minimum (CBM).

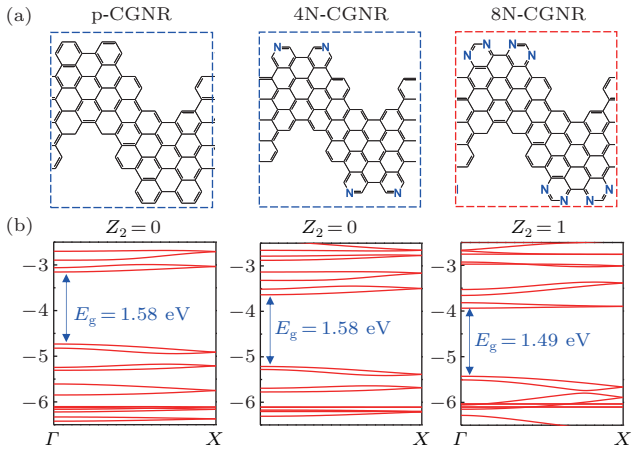


Fig. 1. Electronic properties of chevron GNRs with different topological phases. (a) Schematic and (b) band structures of pristine, 4N-doped and 8N-doped CGNRs.

To investigate the topological properties of CGNRs, the Zak phase of all the occupied π-electron bands for these three CGNRs is considered.[26] The Zak phase of the n-th band is the integral over the BZ of the Berry connection written as

$$\gamma_n = \mathrm{i}\left(\frac{2\pi}{d}\right)\int_{-\pi/d}^{\pi/d} \mathrm{d}k\,\langle u_{n\boldsymbol{k}}|\nabla_{\boldsymbol{k}} u_{n\boldsymbol{k}}\rangle\,,$$

where $\boldsymbol{k}$ is the wave vector, d is the unit cell size, $u_{n\boldsymbol{k}}$ is the periodic part of the Bloch wave function of the n-th band. The Zak phase can be expressed in two components: an intercell part (independent of coordinate origin) and an intracell part. In general, the Zak phase depends on the shape of the unit cell and could take on any value. However, if the system has spatial symmetries such as inversion and/or mirror, the intercell Zak phase of a band is quantized at 0 or π (mod 2π), corresponding to a topological trivial or nontrivial band, respectively. Furthermore, when the origin of the unit cell coincides with the inversion or mirror center, only the intercell Zak phase contributes to the total Zak phase. Since the three CGNRs possess inversion and mirror symmetry, only the intercell Zak phase contributes to the total Zak phase. The intercell Zak phase thus serves as the appropriate quantity to characterize the symmetry-protected topological (SPT) phases in CGNR, and depends on the unit cell choice determined by a structure′s termination geometry.

To simplify the calculations, a Z_2 invariant is employed instead of the Zak phase.[27] The Z_2 invariant and the total Zak phase for GNR systems are related by $(-1)^{z_2} = \mathrm{e}^{\mathrm{i}\sum_n \gamma_n}$, where the sum is taken over the occupied bands. $Z_2 = 1$ indicates a nontrivial topological insulator, while $Z_2 = 0$ indicates a trivial insulator. Given the extremely weak spin–orbit coupling (SOC) of carbon atoms, SOC is neglected in our calculations. As a result, time-reversal symmetry leads to effective spin degeneracy. It is emphasized that the Z_2 refers to the inversion-quantized polarization based on the SSH model. The Z_2 invariants have been calculated for these chevron GNRs with specific unit cell shapes indicated by dashed lines in Fig. 1(a). Calculation results demonstrate that 8N-CGNR belongs to the topological nontrivial class ($Z_2 = 1$, marked by red dashed line), whereas p-CGNR and 4N-CGNR belong to the topological trivial class ($Z_2 = 0$, marked by blue dashed line).

To elucidate the mechanism by which nitrogen dopants affect CGNR topology, we analyze the intracell and intercell coupling of the structure by using SSH model. The CGNR structure can be divided into two components: extension segments (blue patterns in Fig. 2(a)) and the straight AGNR backbone. This configuration creates an effective solid-state analogue of a dimerized *cis*-polyacetylene-like SSH model (Fig. 2(b)). The basic elements of SSH model are an ensemble of equivalent fermion states at each site i of the chain, an intracell coupling t_n between two such states within dimers, and an intercell coupling t_m between states of neighboring dimers. The extension segment corresponds to the intracell coupling t_n, while the AGNR backbone determines the intercell coupling t_m. The band dispersion from coupled topological interface states follows the standard two-band tight-binding form $E(k) = \pm\sqrt{t_n^2 + t_m^2 + 2t_n t_m \cos(k)}$.[28,29] This dispersion relation yields a topological non-trivial phase when $t_n < t_m$ ($Z_2 = 1$) and a topological trivial phase when $t_n > t_m$ ($Z_2 = 0$). The nitrogen atoms' doping positions at the GNR edges primarily affects the intracell coupling t_n. This suggests that the topological phase transition from trivial to nontriv-

ial with increasing nitrogen doping levels correlates with decreased intracell hopping.

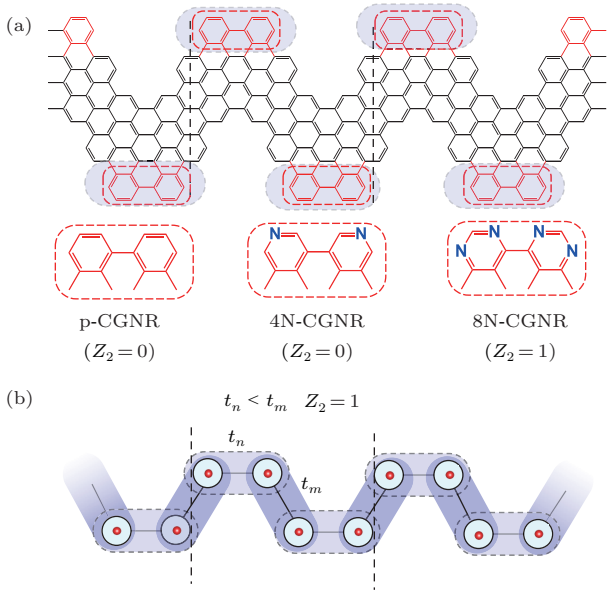


Fig. 2. (a) Schematic structures of chevron nanoribbons with pure carbon, 4 N atoms doped and 8 N atoms doped in a unit cell. (b) Schematic of SSH model.

Furthermore, 8N-CGNR exhibits a 0.2% lattice constant expansion in the x direction (along the periodic direction) and a -2% compression in the y direction (perpendicular to the periodic direction) compared to p-CGNR. This observation indicates that strain influences the topological phase transition in p-CGNR. Figure S1 shows that p-CGNR transforms from trivial to nontrivial one when subjected to tensile (compressive) strain exceeding 20% along the x (y) direction. Specifically, tensile stress along the x direction increases C–C bond lengths in the x direction, indicating decreased intracell coupling t_n. Conversely, compressive stress in the y direction increases intercell coupling t_m. The energy dispersion relation $E(k)$ as a function of t_n and t_m of the p-, 4N- and 8N-CGNRs is displayed in Fig. S2. The results indicate the doping and strain effect both contribute to the reduction of t_n/t_m and triggers the topological phase transition from trivial to nontrivial.

As demonstrated by Cao *et al.*, localized junction states emerged between two GNRs with distinct topological properties.[8] Based on the Z_2 values of CGNRs, a CGNR heterojunction was constructed consisting of two topologically inequivalent segments 4N-CGNR and 8N-CGNR, as illustrated in Fig. 3(a). A superlattice structure with a lattice parameter of 13.7 nm was employed for the 4N-CGNR/8N-CGNR heterojunction. The density of states (DOS) of the heterojunction in Fig. 3(b) reveals a new state emerging at 1.3 eV above the Fermi level. The spatial distribution of this new state is depicted in Fig. 3(c). We find that only π orbitals participate in the formation of states near the band gap. Additionally, the new state localizes at the interface between the two topologically inequivalent segments. This state aligns with the bulk-boundary correspondence principle, confirming its nontrivial heterojunction nature. Notably, Cai *et al.* successfully fabricated a similar CGNR heterojunction on surfaces,[21] suggesting the feasibility of experimental fabrication for the 4N-CGNR/8N-CGNR heterojunction.

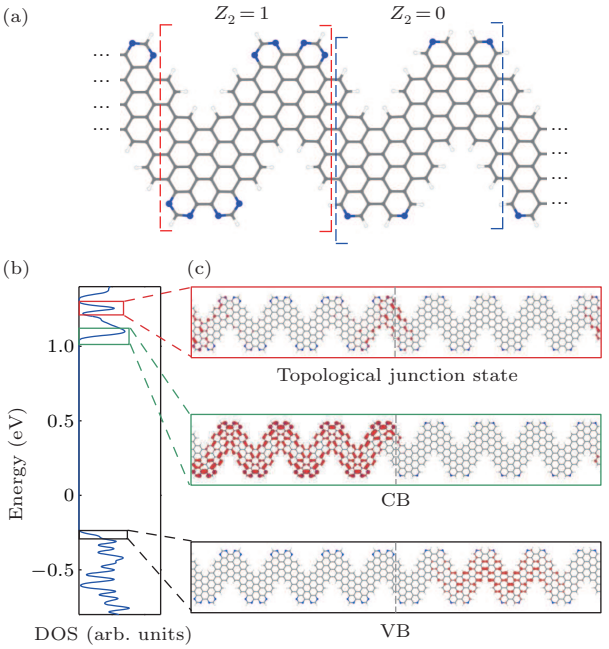


Fig. 3. (a) GNR heterojunctions formed with two topologically inequivalent segments. (b) The density of states of the heterojunctions. The topological junction state, CB and VB are indicated by red, green and black boxes, respectively. The spatial distribution of these three states is shown in panel (c). The iso-surface value of topological junction state, CB and VB are set to be 0.0008 e/Bohr^3.

The nontrivial junction state does not emerge around the Fermi level, potentially due to band alignment between the two semiconductors. Band structure analysis (Fig. S3) indicates that the 4N-CGNR/8N-CGNR heterojunction exhibits type-II band alignment, where the CBM of the heterostructure resides in one material and the VBM in the other. This configuration is confirmed by the spatial distribution of the valence band (VB) and conduction band (CB) of the heterojunction, with VB distributed at the 4N-CGNR and CB at 8N-CGNR (Fig. 3(c)). The presence of heterojunction states around the Fermi level would be advantageous, as topological states could be realized and measured directly without doping. Analysis suggests that heterojunction states are more likely to appear around the Fermi level in type-I band alignment, where both the CBM and VBM reside in the same material.

A type-I band alignment non-trivial heterojunction is designed, wherein the wave functions of the CB and VB states distant from the band gap of the combined systems reside in the bulk region. The results demonstrate the type-I alignment between $L=9$ AGNR (where L represents the number of carbon atom rows forming the ribbon width) and 4N-CGNR, as shown in Fig. 4(a). The DOS emerges from the bulk regions away from the junction. Two states appear near the Fermi

level, indicated by orange shading in Fig. 4(b). These new states constitute topologically induced junction states (JS) localized at the interface between the two topologically inequivalent segments, as shown in Fig. 4(c). For comparative analysis, a type-II band alignment non-trivial heterojunction comprising 9 AGNR and 8N-CGNR is constructed, as depicted in Fig. 4(d). The non-trivial state localizes at the interface between the two topologically inequivalent segments (shown in Fig. 4(f)), emerging at 0.7 eV above the Fermi level (orange shading in Fig. 4(e)). Furthermore, the ground state of the GNR heterojunction consisting of 9AGNR ($Z_2 = 1$) and 4N-CGNR ($Z_2 = 0$) exhibits antiferromagnetism (AFM). According to Lieb's theorem, the antiferromagnetism in the 9AGNR/4N-CGNR heterojunction stems from sublattice imbalance of two carbon atoms.

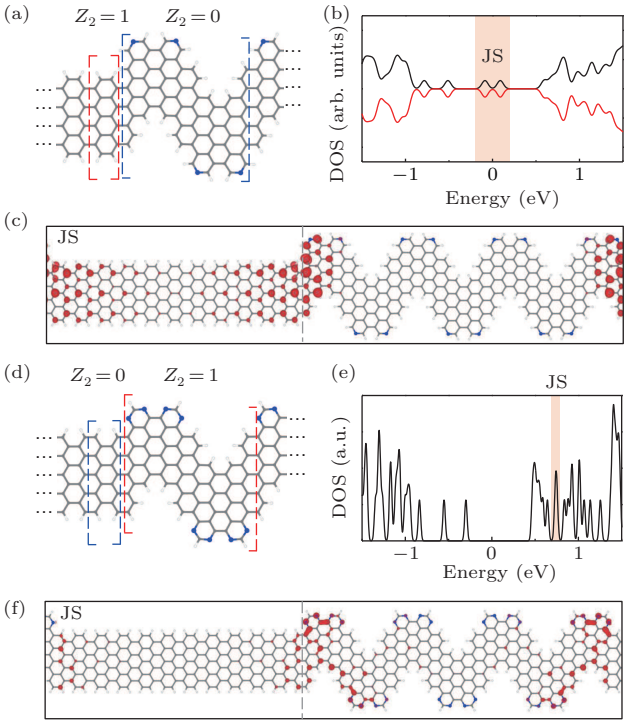


Fig. 4. GNR heterojunctions formed with two topologically inequivalent segments. Heterostructure consisting of (a) 9AGNR /4N-CGNR and (d) 9AGNR /8N-CGNR. The densities of states of the heterojunctions in panels (a) and (d) are shown in panels (b) and (e). The topological junction states are indicated by orange shadow. The spatial distribution of topological junction state (indicated by orange shadow in panels (b) and (d)) is shown in panels (c) and (f). The iso-surface value is set to be 0.001 e/Bohr^3 in panel (c) and 0.0008 e/Bohr^3 in panel (f).

To further investigate the AFM in the structure, we build a 1D AFM spin chain model. When considering the electron spin degree of freedom, the junction states are coupled to each other in a 1D superlattice, forming a 1D AFM spin chain, as illustrated in Fig. 5(a). The interactions between these spin centers generate a 1D Heisenberg-type antiferromagnetic spin 1/2 chain (Fig. 5(b)). The effective exchange interactions between the spin centers are mediated through both the 9 AGNR segment and the 4N-GNR segment. The spin-dependent part of the Hamiltonian can be expressed as

$$H = \Sigma_i \left[J_1 \hat{s}_i^1 \cdot \hat{s}_i^2 + J_2 \hat{s}_i^2 \cdot \hat{s}_{i+1}^1 \right].$$

Here, i denotes the unit cell index of the superlattice, with two spin centers present in each unit cell. To determine the coupling strengths J_1 (through the 9-AGNR segment) and J_2 (through the 4N-CGNR segment) from first-principles calculations, three different spin configurations are analyzed, as shown in Fig. 5(b). Using the total energy differences from our first-principles calculations, we obtain $J_1 = 32.5$ meV and $J_2 = 0.1$ meV.

The exchange parameters were calculated as a function of the distance between the spin centers, denoted as d_1 and d_2, respectively. Figure 5(c) illustrates the relationship between the exchange parameters and distance. The exchange coupling exhibits an exponential decay with distance. All calculated exchange interactions demonstrate positive values, indicating AFM coupling between the spins. Notably, the exchange interaction energy J_1 maintains a significant magnitude of 7 meV, even at a separation distance of 4.8 nm between spin centers. These stable spin centers and their exchange interactions provide a versatile and tunable material platform for investigating novel quantum spin effects in 1D.

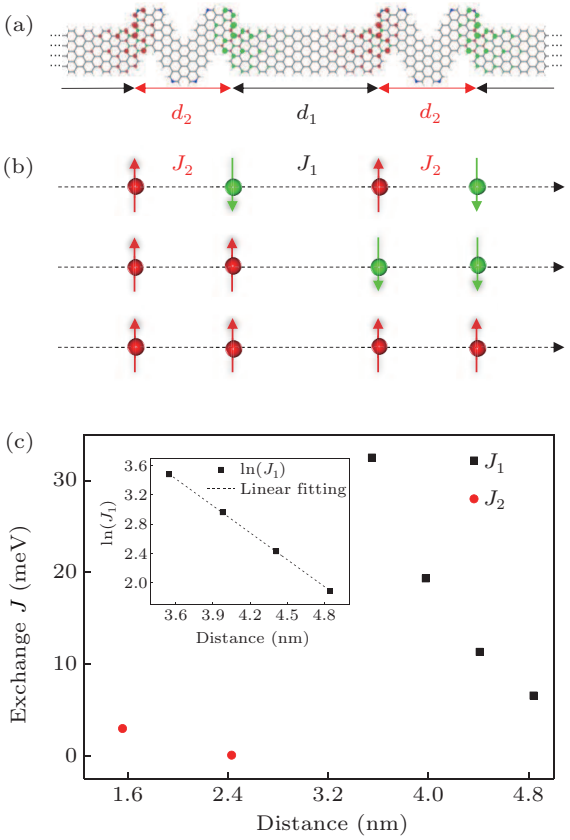


Fig. 5. (a) The spatial distributions of spin-polarized electron density in AFM state, where the iso-surface value is set to 0.002 e/Bohr^3. (b) Schematics of the 1D antiferromagnetic Heisenberg spin 1/2 chain corresponding to the system shown in panel (a) and two additional spin configurations considered in calculations to extract the exchange coupling parameters. (d) Exchange parameters in the Heisenberg model as a function of the separation distance.

3. Conclusion

In conclusion, this study demonstrates that the topological phase of chevron GNR can transition from trivial to nontrivial through nitrogen atoms doping. The introduction of hetero-atoms in GNRs represents a novel approach to expand the classification of topological phases in GNR systems beyond conventional pristine GNRs. Additionally, the research reveals multiple possibilities for designing heterojunctions exhibiting topologically induced AFM junction states. These topological junction states demonstrate significant potential for quantum topological band engineering.

Appendix A: Computational details

The calculations of GNR heterojunctions are carried out by using Vienna *ab initio* simulation package (VASP) with the projector augmented wave (PAW) method.[30,31] A generalized gradient approximation (GGA) in the form of Perdew–Burke–Ernzerhof (PBE) is adopted for the exchange–correlation functional.[32] The wave functions are expanded using a planewave basis set with an energy cutoff of 400 eV, and K-point sampling was done only at the Γ point. The vacuum layer is larger than 15 Å. The atomic geometries of junctions are fully relaxed until the residual forces on each atom are smaller than 0.01 eV/Å.

DFT calculations as implemented in the Quantum Espresso package are used to calculate the Z_2 invariant of the GNRs.[33] Norm-conserving Martin–Troullier pseudopotentials of C, N and H are used.

Acknowledgments

Project supported by the National Natural Science Foundation of China (Grant Nos. 52572063 and 52350322), the Fundamental Research Funds for the Central Universities (Grant Nos. FRF-TP-24-055A and FRF-IDRY-24-007), the 9th Research Institute of China Electronics Technology Group Corporation's open projects (Grant No. 2024SK-003-2), the State Key Lab for Advanced Metals and Materials (Grant Nos. 41601124 and 41601126), and the Beijing Natural Science Foundation (Grant No. L223029). Computational resources were provided by the Beijing Three Axis Space Technology Co. Ltd.

References

[1] Chen Y L, Analytis J G, Chu J H, Liu Z K, Mo S K, Qi X L, Zhang H J, Lu D H, Dai X, Fang Z, Zhang S C, Fisher I R, Hussain Z and Shen Z X 2009 *Science* **325** 178
[2] Teo J C Y, Fu L and Kane C L 2008 *Phys. Rev. B* **78** 045426
[3] Fu L, Kane C L and Mele E J 2007 *Phys. Rev. Lett.* **98** 106803
[4] Hasan M Z and Kane C L 2010 *Rev. Mod. Phys.* **82** 3045
[5] Kou L Z, Ma Y D, Sun Z Q, Heine T and Chen C F 2017 *J. Phys. Chem. Lett.* **8** 1905
[6] Wang X Y, Wang J, Ding H X and Pan M H 2025 *Surf. Sci. Rep.* **80** 100660
[7] Hou Y H, Zhang T, Sun J T, Liu L W, Yao Y G and Wang Y L 2020 *Chin. Phys. B* **29** 097304
[8] Cao T, Zhao F Z and Louie S G 2017 *Phys. Rev. Lett.* **119** 076401
[9] Lee Y L, Zhao F Z, Cao T, Ihm J and Louie S G 2018 *Nano Lett.* **18** 7247
[10] Yu Y, Liu G G, Luo C, Yang W H, Xiao X B and Chen T 2023 *ACS Appl. Nano Mater.* **7** 18299
[11] Jiang J W and Louie S G 2021 *Nano Lett.* **21** 197
[12] Rizzo D J, Veber G, Cao T, Bronner C, Chen T, Zhao F Z, Rodriguez H, Louie S G, Crommie M F and Fischer F R 2018 *Nature* **560** 204
[13] Gröning O, Wang S Y, Yao X L, Pignedoli C A, Barin G B, Daniels C, Cupo A, Meunier V, Feng X L, Narita A, Müllen K, Ruffieux P and Fasel R 2018 *Nature* **560** 209
[14] Lawrence J, Brandimarte P, Berdonces-Layunta A, Mohammed M S G, Grewal A, Leon C C, Sánchez-Portal D and de Oteyza D G 2020 *ACS Nano* **14** 4499
[15] Abdelsalam H, Corona D, Payod R B, Sakr M A S, Abd-Elkader O H, Zhang Q F and Saroka V A 2025 *Nano Lett.* **25** 10594
[16] Rizzo D J, Jiang J W, Joshi D, Veber G, Bronner C, Durr R A, Jacobse P H, Cao T, Kalayjian A, Rodriguez H, Butler P, Chen T, Louie S G, Fischer F R and Crommie M F 2021 *ACS Nano* **15** 20633
[17] Li J C, Sanz S, Merino-Díez N, Vilas-Varela M, Garcia-Lekue A, Corso M, de Oteyza D G, Frederiksen T, Peña D and Pascual J I 2021 *Nat. Commun.* **12** 5538
[18] Lee Y L, Zhao F Z, Cao T, Ihm J and Louie S G 2018 *Nano Lett.* **18** 7247
[19] Lin K S and Chou M Y 2018 *Nano Lett.* **18** 7254
[20] Sun Q, Yan Y Y, Yao X L, Müllen K, Narita A, Fasel R and Ruffieux P 2021 *J. Phys. Chem. Lett.* **12** 8679
[21] Cai J M, Pignedoli C A, Talirz L, Ruffieux P, Sode H, Liang L B, Meunier V, Berger R, Li R J, Feng X L, Mullen K and Fasel R 2014 *Nat. Nanotechnol.* **9** 896
[22] Zhang Y, Zhang Y F, Li G, Lu J C, Lin X, Du S X, Berger R, Feng X L, Mullen K and Gao H J 2014 *Appl. Phys. Lett.* **105** 023101
[23] Vo T H, Perera U G E, Shekhirev M, Pour M M, Kunkel D A, Lu H D, Gruverman A, Sutter E, Cotlet M, Nykypanchuk D, Zahl P, Enders A, Sinitskii A and Sutter P 2015 *Nano Lett.* **15** 5770
[24] Cai J M, Ruffieux P, Jaafar R, Bieri M, Braun T, Blankenburg S, Muoth M, Seitsonen A P, Saleh M, Feng X L, Mullen K and Fasel R 2010 *Nature* **466** 470
[25] Bronner C, Stremlau S, Gille M, Brausse F, Haase A, Hecht S and Tegeder P 2013 *Angew. Chem. Int. Edit.* **52** 4422
[26] Zak J 1989 *Phys. Rev. Lett.* **62** 2747
[27] Fu L and Kane C L 2007 *Phys. Rev. B* **76** 045302
[28] Heeger A J, Kivelson S, Schrieffer J R and Su W P 1988 *Rev. Mod. Phys.* **60** 781
[29] Asbóth J K, Oroszlány L and Pályi A 2016 *Lecture Notes in Physics* Vol. 919
[30] Kresse G and Furthmuller J 1996 *Comp. Mater. Sci.* **6** 15
[31] Kresse G and Furthmuller J 1996 *Phys. Rev. B* **54** 11169
[32] Perdew J P, Burke K and Ernzerhof M 1996 *Phys. Rev. Lett.* **77** 3865
[33] Giannozzi P, Baroni S, Bonini N, Calandra M, Car R, Cavazzoni C, Ceresoli D, Chiarotti G L, Cococcioni M, Dabo I, Dal Corso A, de Gironcoli S, Fabris S, Fratesi G, Gebauer R, Gerstmann U, Gougoussis C, Kokalj A, Lazzeri M, Martin-Samos L, Marzari N, Mauri F, Mazzarello R, Paolini S, Pasquarello A, Paulatto L, Sbraccia C, Scandolo S, Sclauzero G, Seitsonen A P, Smogunov A, Umari P and Wentzcovitch R M 2009 *J Phys-Condens. Mat.* **21** 395502